



Supplementary Materials for

Abrupt CO₂ release to the atmosphere under glacial and early interglacial climate conditions

C. Nehrbass-Ahles*, J. Shin, J. Schmitt, B. Bereiter, F. Joos, A. Schilt, L. Schmidely,
L. Silva, G. Teste, R. Grilli, J. Chappellaz, D. Hodell, H. Fischer, T. F. Stocker

*Corresponding author. Email: cn425@cam.ac.uk

Published 21 August 2020, *Science* **369**, 1000 (2020)
DOI: [10.1126/science.aay8178](https://doi.org/10.1126/science.aay8178)

This PDF file includes:

Materials and Methods
Supplementary Text
Figs. S1 to S9
Table S1
Captions for Data S1 and S2
References

Other Supplementary Material for this manuscript includes the following:
(available at science.sciencemag.org/content/369/6506/1000/suppl/DC1)

Data S1 and S2 (.xlsx)

Materials and Methods

EPICA Dome C CO₂ measurements

The majority of CO₂ measurements on the EPICA Dome C (EDC) ice core were performed at Climate and Environmental Physics (CEP), Physics Institute, University of Bern, Switzerland. The data were measured using the recently developed dry-extraction system, the Centrifugal Ice Microtome (CIM), described in detail in Ref. (56). With this friction-free extraction system, we performed a total of 1161 single measurements with a polar ice sample throughput of up to 24 samples per day. On average, individual ice samples weighed 7.3 ± 0.8 g after approximately 5 mm was trimmed from the outer surfaces. Additionally, we performed 463 control measurements throughout the measurement campaign to correct offsets related to the extraction process and to monitor potential system drifts. These measurements involve expanding a standard gas over a gas-free ice sample that is treated identically to a polar ice sample, and is measured against the same calibration gas (56). Typically, we made one control measurement for every four polar ice samples amounting to five to seven control measurements per measurement day. Over the course of the measurement campaign, which was approximately one year, the mean control measurement was 2.31 ± 1.21 ppm higher than the calibrated value of the reference gas that has been mixed over the gas-free ice. All polar ice measurements have been corrected using the daily average of these control measurements.

All individual depth levels were measured at least in duplicate. For approximately 50% of all samples, a set of vertically contiguous (i.e., directly neighboring) replicate measurements were performed on a different day, leading to a mean sample replication of three samples per final data point. All CIM measurements were grouped (i.e., averaged) to depth sections of usually ~ 5 cm (in rare cases up to 12 cm) in the vertical direction, thereby integrating the signal on average over 23 ± 7 years until 425 ka BP (thousand years before present, where present is defined as 1950 CE), and 60 ± 16 years beyond. In total we provide 387 new data points between 330 and 450 ka BP [i.e., Marine Isotope Stage (MIS) 9e - 12a]. The pooled standard deviation for all replicate samples is 1.0 ppm, which is used as an error estimate for all CIM measurements. All CIM CO₂ measurements are referenced to the WMOX2007 mole fraction scale (57) using four different primary dry air standards calibrated at the NOAA Earth System Research Laboratory, Boulder, USA ranging between 192.44 ± 0.11 and 363.08 ± 0.06 ppm CO₂.

An additional 33 measurements between 297 and 353 ka BP were performed at the Institut des Géosciences de l'Environnement (IGE), Univ. Grenoble Alpes, France using the Ball Mill extraction technique described in detail in Ref. (58). Here, larger samples of 42.5 ± 2.5 g were used. The extracted air of each sample is analyzed five consecutive times (i.e., in total five sample injections into the gas analyzer). The precision of the system amounts to an average of ~ 1.7 ppm and is based on the standard deviation of these five injections, thus does not include the additional extraction variability of replicate samples. The CO₂ measurements are calibrated using a working standard (233.7 ± 0.4 ppm CO₂, synthetic dry air provided by Air Liquide, Grenoble, France), which has been referenced to two primary dry air standards with calibrated CO₂ mole fractions of 238.34 ± 0.04 ppm and 260.26 ± 0.20 ppm, provided by the NOAA Earth System Research Laboratory, Boulder, USA and the Commonwealth Scientific and Industrial Research Organisation (CSIRO), Australia, respectively.

Gas ages for all CO₂ measurements produced by the CIM and Ball Mill were calculated using the average depth levels of each depth section using the AICC2012 chronology (34). We do not find any significant inter-laboratory offset; however, this comparison is only based on 11 directly neighboring samples. Note that due to their lower temporal resolution, the Ball Mill data younger than 328 ka BP are not shown in Fig. 1B and Fig. 2D. All CO₂ data are available in Data S1.

EPICA Dome C CH₄ measurements and compilation of CH₄ data

The existing CH₄ record for MIS 9e - 12a consists of measurements from two experimental setups, one employed at CEP, the other at IGE (21). Here we improve the temporal resolution using the same experimental setups. A total of 92 unpublished CH₄ data points had been produced in 2008 using the CEP setup, within the scope of the work by Ref. (59), but remained unpublished. The method used for these samples is identical to that described in Ref. (21). Secondly, we performed 41 new measurements at IGE at time periods of abrupt climate change connected to Carbon Dioxide Jump (CDJ) events in the CO₂ record. In previous publications, an offset correction between the IGE and CEP setups involved adding 6 ppb to the IGE data (60). This correction is obsolete for the new IGE data as an improved contamination correction has been introduced, removing the interlaboratory offset. Lastly, we complement the above described data with 54 published data points by Ref. (61), that have been measured at CEP; however, with an independent setup. A visual overview of this data can be found in Fig. S2. All CH₄ data are available in Data S1.

The majority of the 92 CH₄ data points produced by Ref. (59) are vertically contiguous (i.e., directly neighboring) to those published by Ref. (21) and should be considered replicate measurements. In our CH₄ compilation (Data S1), we combine two individual measurements to one data point in cases where the vertical depth difference between two neighboring CH₄ data points is smaller than 10 cm (typically less than 5 cm). This entails a CH₄ signal integration over 28±14 years on average, which is less than the smoothing resulting from the firn column (see below). The uncertainty of these averaged values is calculated using Gaussian error propagation. We use this CH₄ compilation in all figures showing EDC CH₄ data in MIS 9e - 12a, with the exception of Fig. S2B where the full data set is shown.

Ocean sediment data from IODP Site U1385 (Shackleton site, Iberian Margin)

Isotope data from the International Ocean Discovery Program (IODP) Site U1385 between 329 and 407 ka BP were measured on the planktic foraminifera *G. bulloides* (Fig. 2H) and epibenthic species belonging to the genus *Cibicidoides* (Fig. 2C, 2I). A condensed section or hiatus in the sedimentation rate in older sections covering MIS 11c - e prevents us from reconstructing hydrographic changes on centennial time scales (62). Most analyses were made on *C. wuellerstorfi* but when this species was rare, other species were used for benthic $\delta^{18}\text{O}$ (i.e., *C. mundulus*, *C. robertsonianus*) (Fig. 2C). Only *C. wuellerstorfi* data are presented for benthic $\delta^{13}\text{C}$ (Fig. 2I) because other species may live infaunally and therefore do not record the $\delta^{13}\text{C}$ signal of the bottom water. All measurements were made at the Godwin Laboratory of Palaeoclimate Research, University of Cambridge, UK using the same methods as those described in Ref. (62). All marine sediment data are available in Data S2.

Piston cores from the Iberian Margin off Portugal contain clear signals of millennial variability of both surface and deep-water masses (28, 63). Variations in planktic $\delta^{18}\text{O}$ and alkenone saturation index ($U^{K'_{37}}$) reflect the temperature variations in Greenland over the last glacial cycle (64). In the same sediment core, the benthic $\delta^{18}\text{O}$ signal resembles the δD record in Antarctica ice cores (28, 63) capturing each of the Antarctic Isotope Maxima events during the last glaciation (10). Millennial variations in benthic $\delta^{18}\text{O}$ are affected by changes in deep-water temperature and water mass hydrography, and are assumed to be a signal that originates from the Southern Ocean (SO) (28, 65). We synchronized IODP Site U1385 with EDC on the AICC2012 age scale (34) by correlating the benthic $\delta^{18}\text{O}$ and δD records (Fig. 2C, 2A) (cf. 66, 67). This correlation results in agreement between the planktic $\delta^{18}\text{O}$ record and the CH_4 compilation (Fig. 2H, 2E). The observed phasing of the planktic and benthic $\delta^{18}\text{O}$ signals at IODP Site U1385 is consistent with the relative changes in temperature between Antarctica and Greenland deduced from CH_4 synchronization.

Gravitational correction of the CO_2 and CH_4 data

Before small samples of the atmosphere become trapped in the ice, the air first needs to diffuse through the firn column of a polar ice sheet. Under the influence of the Earth's gravitational field heavier molecules become enriched compared to the air that entered the firn at the surface of the ice sheet (68), while lighter molecules become depleted. This process is commonly referred to as gravitational settling. The magnitude of this effect is dependent on the thickness of the diffusive firn column and therefore varies with changing temperature and accumulation rates. Atmospheric $\delta^{15}\text{N}_2$ (the isotopic signal of N_2) can be safely assumed to be constant over orbital time scales, which makes the $\delta^{15}\text{N}_2$ of the air trapped in the ice an ideal tracer of gravitational effects and can also be used to correct for other gas species that are subject to change in the atmosphere, such as CO_2 and CH_4 (69, 70).

With approximately 44 g mol^{-1} CO_2 is heavier than the mean molar weight of air, which amounts to 29 g mol^{-1} causing slightly higher CO_2 mole fractions where bubble formation takes place. With 16 g mol^{-1} CH_4 is lighter than air leading to slightly lower CH_4 mole fractions at bubble close off. While the correction of such effects is vital for reconstructions of stable isotopic ratios (e.g., 29), it was not systematically corrected for in previous studies solely focusing on mole fractions, as the effect is only on the order of 1% of the measured value.

Although this systematic bias is well known, many authors refrained from applying this correction, possibly due to the lack of $\delta^{15}\text{N}_2$ data (or similar proxies) or the generally small magnitude of the correction which often was smaller than the measurement precision. However, with steadily increasing technical capabilities and a growing body of $\delta^{15}\text{N}_2$ data the above raised arguments are obsolete. In particular, with respect to the accumulating evidence for systematic non-trivial offsets between different CO_2 reconstructions this correction is necessary (4, 71).

To estimate the gravitational correction for EDC data, we use $\delta^{15}\text{N}_2$ measurements published by Ref. (72). For each of our data points, we find the corresponding EDC δD value by linear approximation of the δD data set published by Ref. (10). Subsequently, we make use of the linear relationship between δD and $\delta^{15}\text{N}_2$ to approximate our $\delta^{15}\text{N}_2$ as previously proposed by Ref. (29). The Vostok data shown in Fig. S2A are corrected using

a linear regression between δD (10) and $\delta^{15}N_2$ (73). The additional error introduced by this correction is negligible compared to the experimental errors of the CO₂ mole fractions. The gravitational correction for our measurements involves reducing the uncorrected CO₂ data by 1.1 to 2.5 ppm and adding between 2 and 6 ppb to the CH₄ data.

Note that all CO₂ and CH₄ values shown in Fig. 1, 2, 3, S1, and S2 are corrected for gravitational effects. In order to provide CO₂ mole fractions that are consistent with previously published CO₂ compilations where gravitational corrections have not been consistently applied (74, 75), we also provide uncorrected CO₂ and CH₄ data in Data S1.

Calculating the rate of CO₂ and CH₄ change in the ice core record

To calculate rate of change in CO₂ (Fig. 1D) on centennial to millennial timescales, superimposed orbital trends have to be removed from the data set first (cf. 67). This is achieved by subtracting a smoothing spline from the data set (76), with cut-off periods (i.e., degrees of smoothing) ranging from 6 to 14 ka (Fig. S3A). Subsequently, we use a second set of smoothing splines with cut-off periods ranging from 0.4 to 1.2 ka to interpolate these detrended data to obtain annually resolved equidistant records (Fig. S3B - F). These interpolated data are used to calculate central finite differences to approximate the first derivative of these CO₂ records (Fig. S3G - K). For the removal of orbital scale variability, we choose the 10 ka cut-off period smoothing function, which is a compromise between preserving sub-millennial scale variability while removing the orbital-scale glacial-interglacial trends. The interpolation of the detrended data is done using a 0.8 ka cut-off period smoothing function, which is a compromise between the amplification of high-frequency noise and loss of signal amplitude of potential CDJ events (cf. 67). The same methodology is used for calculating the rate of change in the CH₄ record (Fig. 1E).

Estimating realistic Gas Age Distributions for the EDC ice core

The air trapped at a particular depth of the ice core is a mixture over decades to millennia depending on accumulation rate and site temperature (77). The atmospheric air diffuses through the firn column and mixes with older air masses before it gets trapped in the ice. Most importantly, bubbles in the firn-ice transition (lock-in) zone close off slowly and not at the same time which leads to an attenuation or low-pass filtering of the atmospheric signal (78, 79). This process scales with the time it takes a single layer of firn/ice to pass through the lock-in zone. The age difference (delta age) between the ice and the mean age of the gas trapped within the ice is a first-order indicator of average accumulation rates over the entire firn column. With decreasing accumulation these effects become more pronounced, leading to a particularly strong signal attenuation and multi-millennial delta ages in the Vostok and EDC ice core that are from low-accumulation sites located on the Antarctic Plateau. The age of the enclosed air after this firn column-induced smoothing is described by a probability density function. It is often referred to as the Gas Age Distribution (GAD), and its width is different for each depth section depending on past accumulation rates and temperatures. Figure S4 shows three typical shapes (blue lines) of commonly used GAD for the EDC ice core (78, 80), which are representative for warm interglacial (pre-industrial), deglacial [Bølling-Allerød (BA)], and cold glacial conditions (Last Glacial Maximum), respectively.

Recently, Ref. (81) described an empirical method to estimate GAD for the Vostok ice core based on the direct comparison between continuously measured CH₄ records. This

method involves finding a generic GAD that convolves the high-frequency CH₄ signal captured by the West Antarctic Ice Sheet Divide (WD) ice core (18) at points of fast CH₄ transitions (in their case DO 17 at ~59 ka BP) to match the smoothed version of the identical atmospheric signal in the Vostok ice core. The assumption is made that the continuous WD CH₄ record provides an insignificantly smoothed version of the atmospheric signal (6). Ref. (81) raised concern that commonly used modelled estimates of GAD for low-accumulation sites during glacial conditions may be systematically too wide. Consequently, such GAD would lead to a systematic overestimation of the firn column-induced smoothing effect. However, it is yet unknown whether this finding is unique to the Vostok ice core under glacial conditions or whether interglacial GAD estimates are affected in a similar way. Moreover, it is not clear – although likely – whether this applies to other ice cores with similar temperature and accumulation regimes, such as the EDC ice core.

Indirect evidence that commonly used GAD for the EDC ice core (78) are too wide comes from a study by Ref. (80). They estimated the atmospheric CO₂ rise rates for the CDJ+ found at the onset of the BA period (9) using a GAD similar to that predicted by Ref. (78) (Fig. S4). By comparison with the WD CO₂ record, their estimations were later shown to be clear overestimations of the atmospheric rise rates (6), which can be explained by the usage of a too wide GAD in the study by Ref. (80).

Following the techniques described in Ref. (81), it is possible to test the commonly used modelled GAD (78) in the case of the EDC ice core. The WD CH₄ record is available at decadal resolution for the period between 10 and 67 ka BP (18), where only discretely measured data are available from the EDC ice core (21). In comparison to a continuous record, this record is much lower in resolution (approx. 160 years between 10 and 67 ka BP on average) and suffers from staggered layering artefacts (centimeter-scale age scale reversions) that cannot be unambiguously identified in a non-continuous record (81, 82). Furthermore, all measurements over MIS 3 predating ~30 ka BP are located in the brittle ice zone of the EDC ice core, which is prone to sample contamination by drilling fluid and modern air.

Nevertheless, the discrete EDC CH₄ data are sufficient to construct a first-order approximation of a more realistic GAD. Here, we focus on the onsets of three key periods that are associated with fast atmospheric CH₄ rises, namely the Preboreal (PB), Younger Dryas (YD), and the BA. In addition, we also include Dansgaard-Oeschger (DO) events 6 - 8 between 33 and 39 ka BP (Fig. S5) associated with a major CH₄ rise for each DO event. Together with the data available for the last deglaciation (10 to 22 ka BP), this interval has the highest temporal resolution (~100 years) in the 10 to 67 ka BP interval where continuous WD CH₄ data are available (18). We assume that the GAD can be approximated by log-normal distributions (80, 81) and that a single GAD is representative for the enclosure characteristics for these events. Log-normal functions are described by two free parameters: the mean (μ) and standard deviation (σ) of the logarithm. For the sake of simplicity, we fix the standard deviation at a value of $\sigma=1.5$ (81) and vary only the mean to change the shape of our GAD. We also report the arithmetic mean of the log-normal function [referred to as expected mean in Ref. (80)] representing the width of the GAD, given in years (Table S1). The arithmetic mean of a log-normal distribution is given by

$$GAD_{mean} = e^{\mu+0.5\sigma^2}. \quad \text{Eq. S1}$$

We use the *fminbnd* function of the ‘neldermead’ package in R (83) to optimize the EDC bubble enclosure characteristics by smoothing the WD CH₄ data (18) to fit the EDC data (21). The optimal GAD is determined by minimizing the root-mean-square error (RMSE) between the convoluted WD CH₄ signal and the discrete EDC data, spanning a 2 ka time window centered around the inflection point of the abrupt CH₄ rise in the EDC record (Fig. S5). We allow for linear adjustments of the discrete EDC data relative to the continuous WD CH₄ data to compensate for the temporal shift induced by the convolution of the WD CH₄ signal (80), as well as general age scale and standardization inconsistencies. To acknowledge the dependency on the absolute value of individual data points we apply a Monte Carlo type approach and vary the discrete CH₄ data within their uncertainty boundaries (± 10 ppb) in a random manner. We use the average of 500 iterations to determine the most suitable GAD width for each event. In this context the choice of age scale is critical, as it has a strong influence on the duration of an event. Therefore, we use the age scale as published by Ref. (84) that has been specifically optimized for the deglaciation period and includes the PB, YD, and BA events. Note that for all other purposes the AICC2012 age scale is used (34). For the glacial GAD – as represented by DO 6 - 8 between 33 and 39 ka BP – three events are optimized simultaneously to compensate for the influence of age scale inconsistencies between the AICC2012 (discrete EDC CH₄ data) (34) and the WD2014 age scale (continuous WD CH₄ data) (85) and minimize the influence of potential staggered layering artefacts (18, 81) in this section (Fig. S5).

The smoothed versions of the WD CH₄ record match the discrete EDC CH₄ data well for all three events during the deglaciation (Fig. S5). In the case of DO 6 - 8 the size of each event in the discrete EDC data is well captured by the smoothed version of the WD CH₄ record, despite obvious age scales issues, indicated by relative shifts between the discrete and smoothed continuous records. The results of this optimization (Fig. S4, S5) point towards a substantial overestimation of the smoothing produced by commonly used modelled EDC enclosure characteristics (78), in line with Ref. (81).

Since these four time periods are only representative for a given firm column condition, we strive to find a simple model that allows to estimate the GAD width (Eq. S1) for other firm column conditions at Dome C, as approximated by the delta age. Therefore, we plot the arithmetic means of the GAD found for the PB, YD, BA, and DO 6 - 8 against their respective delta age to the nearest 0.1 ka (Fig. S6). Delta ages are derived from the AICC2012 age scale (34) by subtracting the assigned gas age from the respective ice age for each depth interval. We use a 2 ka time window centered around the inflection point of each event to find the corresponding average delta age given on the ice age scale. Subsequently, a linear regression model incorporating the uncertainties for both variables (86) is utilized to obtain the following empirical relationship:

$$GAD_{mean} = 0.048(\pm 0.025) \times \text{delta age (in years)} + 17(\pm 67) \text{ years.} \quad \text{Eq. S2}$$

This linear function serves as a first-order approximation of more realistic GAD for the EDC ice core, assuming a linear scaling of the GAD width with delta age.

We stress that these GAD estimates are limited in several aspects. Most importantly, these estimates are highly dependent on the used age scale, as the duration of fast CH₄ transitions and the delta age estimate may vary considerably. Also the choice of the GAD template (here a log-normal distribution) might have an influence on the

quantitative outcome of this analysis. However, the good correspondence of the WD record smoothed by a log-normal GAD with the measured EDC record strongly suggests that such an influence does not affect the overall conclusions of our study. We recommend that this case study is repeated when higher resolution data from the EDC ice core for selected time periods of fast atmospheric CH₄ change and improved empiric GAD information become available.

Inversed convolution of Carbon Dioxide Jumps

The rates of CO₂ increase archived in the ice core record during CDJ can only be interpreted as lower limits for the unfiltered atmospheric rates. Independent of the original atmospheric trajectory, the growth rates in atmospheric CO₂ must have been higher than recorded in the smoothed ice core record. It is therefore important to consider the air enclosure characteristics of the EDC ice core when attempting to deconvolute the ice core signal and estimate potential atmospheric rates.

Using our GAD estimates for the EDC ice core derived as described above, we provide first-order estimates of atmospheric duration, magnitude of the CO₂ rise, and growth rates for each event identified here. To achieve this, we assume that the centennial to millennial-scale atmospheric trajectories can be approximated by a simple set of linear functions. Our atmospheric rates are estimated following these steps: (i) Find the delta age for the CDJ using the AICC2012 age scale (34); (ii) determine a suitable GAD using the linear relationship described above; (iii) guess a simple atmospheric trajectory, smooth this guess using the GAD, calculate RMSE between smoothed guess and the actual CO₂ data, and optimize this atmospheric guess using the Nelder-Mead algorithm; (iv) repeat step (iii) 200 times with randomly modified CO₂ record within the measurement uncertainty (± 1 ppm); (v) calculate the median values for the duration, magnitude of the CO₂ rise, and growth rates for each CDJ of these 200 iterations, as indicated by blue segments in Fig. 3B and S1B. The results are shown in Table S1, where the interquartile range of these 200 iterations is used as an error estimate.

Supplementary Text

Comparison of the new CO₂ data set with previously published records

Our new EDC CO₂ data overall agree with the published Vostok 5G measurements [Fig. S2A, (1)]. Differences in the two records can be explained by age scale uncertainties beyond 355 ka BP due to the lack of stratigraphic tie points in the Vostok record, leading to inconsistencies of up to ~ 10 ka (33, 34). During MIS 11c - e (~ 390 to 430 ka BP) our data agree well with the data published by Ref. (2) measured on the same ice core. No difference in average mole fractions is found; however, the precision of our new data has been increased substantially. Towards MIS 12a our new data develops an offset with respect to the data published by Ref. (2). Based on the time interval between 438 and 446 ka BP, where CO₂ appears to be stable at a level of 196.2 ± 0.7 ppm (CIM measurements), we determine an offset of 3.5 ± 1.4 ppm between the record published by Ref. (2) and our new CIM data, with our data showing lower mole fractions. Such offsets between different Antarctic records are well known, but still lack a coherent explanation and responsible mechanisms are hard to distinguish from each other (4, 71). However, the majority of mechanisms cause the CO₂ mole fractions to increase over time, for example due to preferential loss of oxygen during storage of the samples (4, 71). The only known

effects that lead to lower CO₂ measurements are related to the combination of measurement setups with low extraction efficiencies and ice from either the so called Bubble to Clathrate Transition Zone (58, 87) or from depth sections in EDC deeper than 3000 m (74). Both mechanisms can be excluded here. Instead, we speculate that the offset is an issue related to standardization methods. While the new data were calibrated using standard reference gases ranging between 192 and 363 ppm (see Materials and Methods), Ref. (2) used air standards only ranging between 252 and 342 ppm (cf. 9), i.e., the lowest concentration standard was still about 50 ppm higher than the lowest measured ice core mole fraction during MIS 12a. In any case, this small glacial offset between the new and older EDC data from this time interval does not affect any of the conclusions drawn in our study.

Estimating the detection limit for CDJ during MIS 9e - 12a in the EPICA Dome C ice core

The absence of CDJ (according to our CDJ definition in the main text) between MIS 10a and late MIS 11a (~345 to 370 ka BP) as well as between early MIS 11e and MIS 12a (~430 to 445 ka BP) raises the question of whether no CDJ events occurred during these periods or if we are only unable to detect them.

It is possible that we do not detect potential CDJ that are smaller than a certain threshold due to the firn column-induced attenuation of the original atmospheric signal. This smoothing effect is strongest for the glacial maxima when temperatures and accumulation rates are at their lowest. Besides the amount of firn smoothing, the detection limit for CDJ in our CO₂ record also depends on the original atmospheric rates and durations of carbon releases to the atmosphere.

We simulate the resulting rate of change of CO₂ as it would be recorded in the EDC ice core (cf. Fig. 1D, 3D, S1D) by smoothing generic CDJ (i.e., simple step functions) and subsequently calculating their rate of change using the same methodology as described above (Fig. S7). We use the maximum firn column-induced smoothing in the MIS 9e - 12a interval, which is found for the glacial maximum during MIS 12a when the delta age reaches its maximum at 4.5 ± 0.3 ka (34) resulting in an arithmetic mean of 233 ± 132 years (Eq. S2) for the GAD used here.

Figure S8 demonstrates the influence of both the simulated magnitude of the CO₂ rise (rows) and event duration (columns) in the atmosphere on the estimated growth rates of a CDJ event as it would be recorded by ice core record, whereas Fig. S7 visualizes the impact of different magnitudes of the CO₂ rise at a fixed CDJ duration (Fig. S7A - C) and *vice versa* (Fig. S7D - F).

Other factors – such as sample availability – may also influence the theoretical detection limit, which can lead to the overestimation of the estimated CDJ duration and underestimation of the determined atmospheric CO₂ rise and growth rate. This may be the case for CDJ– 11a.2, CDJ+ 11a.3, and CDJ+ 11e (Fig. S1). In case of CDJ+ 11e – where we exploited all available ice in this depth section – the CH₄ data suggest a later onset of the CDJ by ~100 years (i.e., a shorter duration) than we estimate based on the inverse convolution of the ice core signal (Table S1). The low ice availability is a result of earlier sampling (e.g., 2, 21, 61) and generally lower ice availability due to low-accumulation rates during the MIS 12a - 11e transition (Termination V) in the EDC ice core. While the majority of our CO₂ dataset is only marginally affected by limited sample availability, we cannot exclude that potential CDJ with CO₂ rises greater than ~5 ppm remain undetected during the MIS 12a - 11e transition.

In summary, based on the above theoretical considerations we should be able to detect CDJ with an atmospheric CO₂ rises greater than ~5 ppm and a duration of less than ~250 years throughout MIS 9e - 11e, i.e., the majority of our record. The finding is supported by the identification of the third largest CDJ of all eight CDJ identified in this study (CDJ- 10a; Table S1), which takes place among the coldest conditions during the entire MIS 10a - 11a glacial period. Consequently, CDJ- 10a is associated with more pronounced firn column-induced smoothing of the atmospheric signal as compared to the preceding MIS 10b to late MIS 11a interval (i.e., ~345 to 370 ka BP) where no CDJ are found (Fig. 1), confirming that we do capture major CDJ even when the firn column-induced signal attenuation is relatively strong.

We speculate that CDJ+ become less likely with decreasing temperatures during a glacial period based on previously published lower precision CO₂ data. We assume that at least four CDJ+ occurred during MIS 5a - c associated with DO 19 - 21 and DO 24 based on apparent jumps in the CO₂ trajectories at the time of sharp CH₄ rises (4, 8), but no robust conclusion can be drawn from these data. With advancing glacial conditions (i.e., decreasing temperatures and lower sea levels) towards MIS 3 the climatic conditions seem to no longer permit the formation of major CDJ+ (4, 5, 8). A single CDJ- associated with Heinrich Stadial (HS) 4 (12, 13) is the only CDJ identified for the MIS 3 interval so far, with no indications of CDJ+ associated with major Carbon Dioxide Maxima (CDM) 4, 8, 12, 14, and 17 (numbering refers to the associated DO event) (4, 8). With the onset of the last deglaciation connected with rising temperatures and sea level, both types of CDJ seem to become more likely again (6, 30). It is thus conceivable that the climatic boundary conditions found during the early glacial growth phases (e.g., MIS 11a, MIS 5a - c) are favorable conditions for the formation of CDJ+ events, that seem to cease towards the coldest conditions reached during the glacial maxima of each glacial cycle (e.g., MIS 10, MIS 3). CDJ-, on the other hand, seem to depend on specific conditions potentially triggered by major freshwater forcing.

CH₄ excursions during Heinrich Stadials in the EPICA Dome C ice core

By comparison with the CDJ- found for HS1 (6) and HS4 (12), we would expect to find simultaneous short-lived overshoots in the CH₄ record, with amplitudes of less than ~50 ppb (18). However, the CDJ- identified here (i.e., CDJ- 10a, 11a2, 11c) show no indication of such signals in the CH₄ data.

We argue that such events cannot be resolved with currently available discrete EDC CH₄ data. This statement is based on considerations for the known events for HS1 and HS4 (18), that are smoothed using our linear model for delta age dependent GAD (Fig. S9). In both cases the short-lived CH₄ overshoot is attenuated to a level that cannot be detected in the EDC ice core, at least by using the discrete CH₄ data from Ref. (21), due to insufficient temporal resolution and measurement precision. This is in line with Ref. (81), who showed that comparable sub-centennial-scale CH₄ variations around DO 17 in the WD CH₄ record are smoothed out in the Vostok ice core.

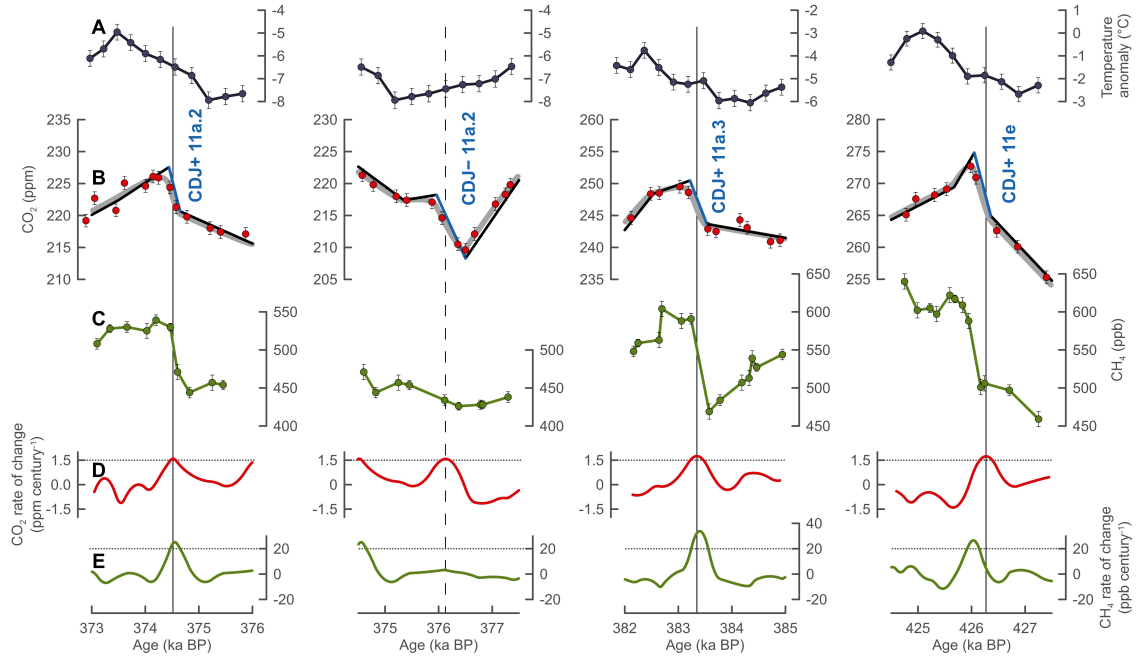


Fig. S1. Extension of Fig. 3. Detailed view of the two varieties of Carbon Dioxide Jumps (CDJ) in the EPICA Dome C (EDC) ice core. (A) EDC temperature anomalies (10) (B) CO₂ data (this study). (C) CH₄ compilation (this study, see materials and methods for details). (D) Rate of change in CO₂ (cf. Fig. 1D). (E) Rate of change in CH₄ (cf. Fig. 1E). CDJ+ are coeval with DO-like CH₄ rises greater 50 ppb at growth rates greater than 20 ppb per century (D), whereas CDJ- are not. The black linear segments in (B) indicate first-order approximations of the atmospheric CO₂ evolution. The blue segment highlights the actual CDJ event. These approximations for the atmospheric trajectories are optimized so that the CO₂ curve after smoothing by the bubble enclosure process (gray lines) fit the ice core data (red points) best. The firm smoothing is realized by applying improved gas enclosure characteristics for the EDC ice core (Fig. S4 - S6). See Table S1 for details. All remaining CDJ are shown in Fig. 3.

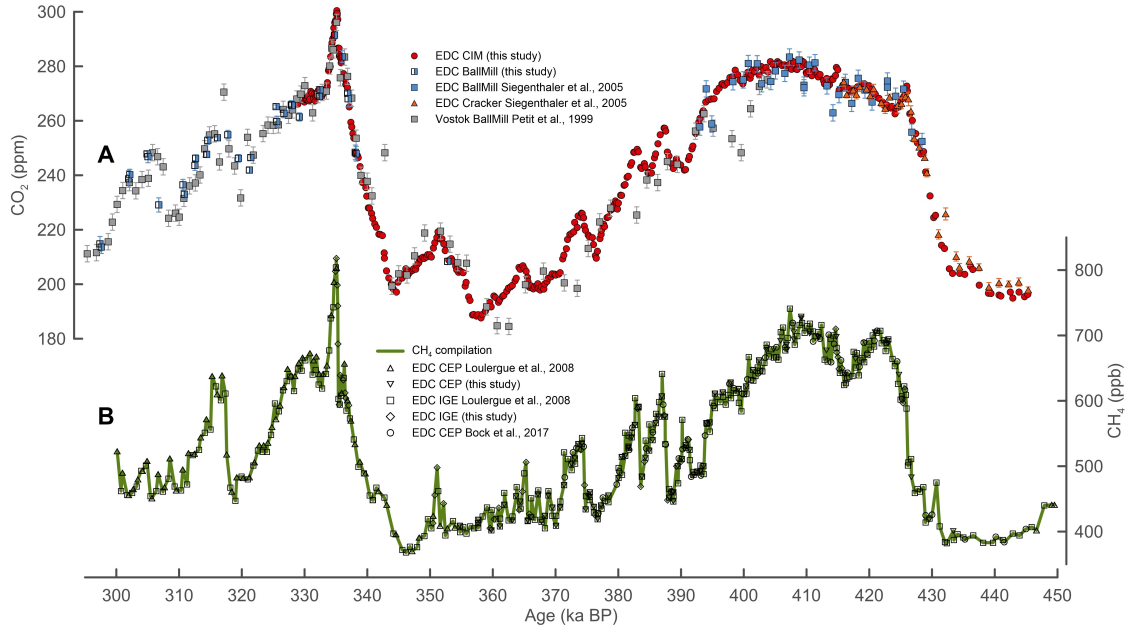


Fig. S2. Comparison between our CO₂ and CH₄ data from the EPICA Dome C (EDC) ice core with previously published data. (A) The new EDC CO₂ record overlaps with CO₂ data from the Vostok 5G ice core during 300 to 400 ka BP (1) and with previously published data from EDC during 390 to 450 ka BP (2). Note that the CO₂ data sets shown here were measured using three different dry extraction devices, namely the Centrifugal Ice Microtome (CIM) (this study) and the Needle Cracker (2) employed at Climate and Environmental Physics (CEP), Physics Institute, University of Bern and the Ball Mill (this study, 1,2) employed at the Institut des Géosciences de l'Environnement (IGE), Univ. Grenoble Alpes. **(B)** EDC CH₄ data, mainly based on data published by Ref. (21), complemented with new measurements (this study) and previously published data (61), all measured at CEP and IGE. Error bars for CH₄ are omitted for clarity. See legends for details.

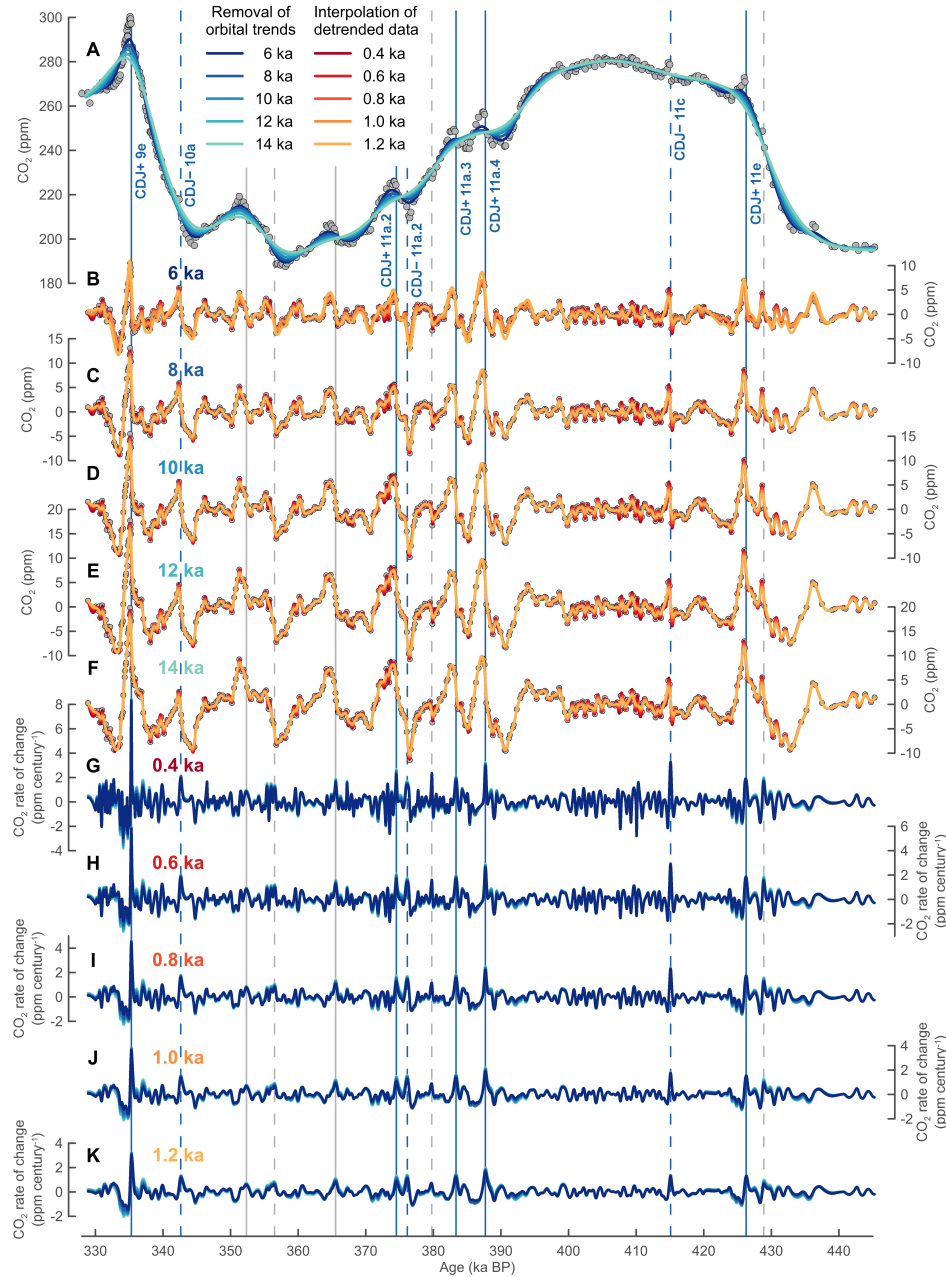


Fig. S3. Calculating the rate of change for our CO₂ record from the EPICA Dome C (EDC) ice core. (A) Removal of orbital to multi-millennial trends from the EDC CO₂ record (gray dots, this study) using five different smoothing splines (76) with cut-off periods (i.e., degrees of smoothing) ranging from 6 to 14 ka. (B-F) Detrended EDC CO₂ record after subtraction of splines shown in (A). A second set of five smoothing splines with cut-off periods ranging from 0.4 to 1.2 ka is applied onto the different detrended data sets, resulting in five times five annually resolved equidistant records containing only the centennial-scale variability. (G-K) Resulting rates of change of the detrended and interpolated CO₂ data from (B-F), grouped by their variant of spline interpolation. See legends for color-coding. Labelling and vertical lines are identical to Fig. 1.

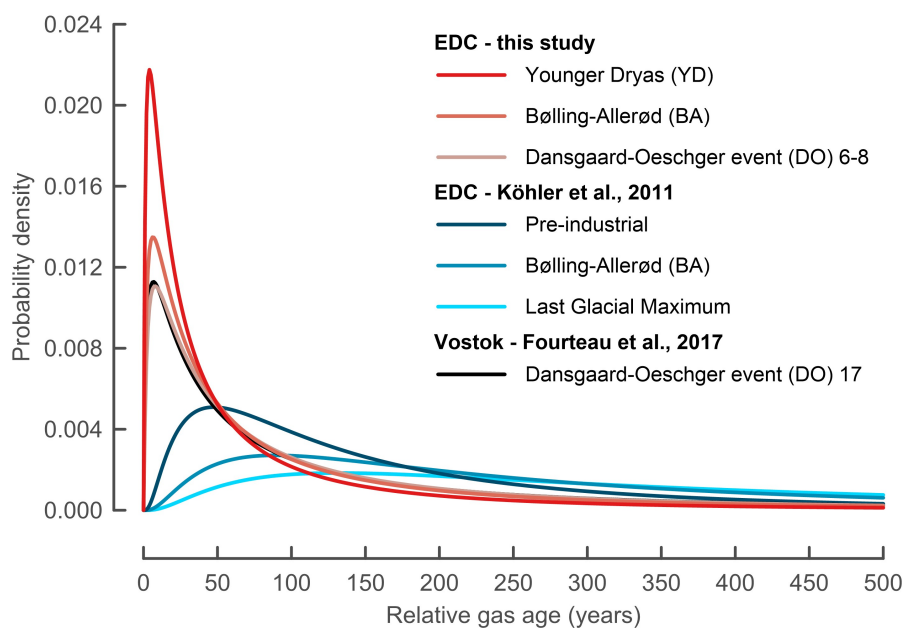


Fig. S4. Gas Age Distributions (GAD) for the low-accumulation sites EPICA Dome C (EDC) and Vostok for different climatic boundary conditions. All GAD shown here are represented by log-normal functions. The scenarios by Ref. (80) are approximations for the firn model outputs by Ref. (78), while our estimates are based on empirical smoothing of the West Antarctic Ice Sheet Divide (WD) CH₄ record to resemble the effective EDC CH₄ measurements (cf. Fig. S5, S6). The estimated GAD for the Preboreal (PB) is nearly congruent with the GAD for the Younger Dryas (YD) event and is omitted for clarity.

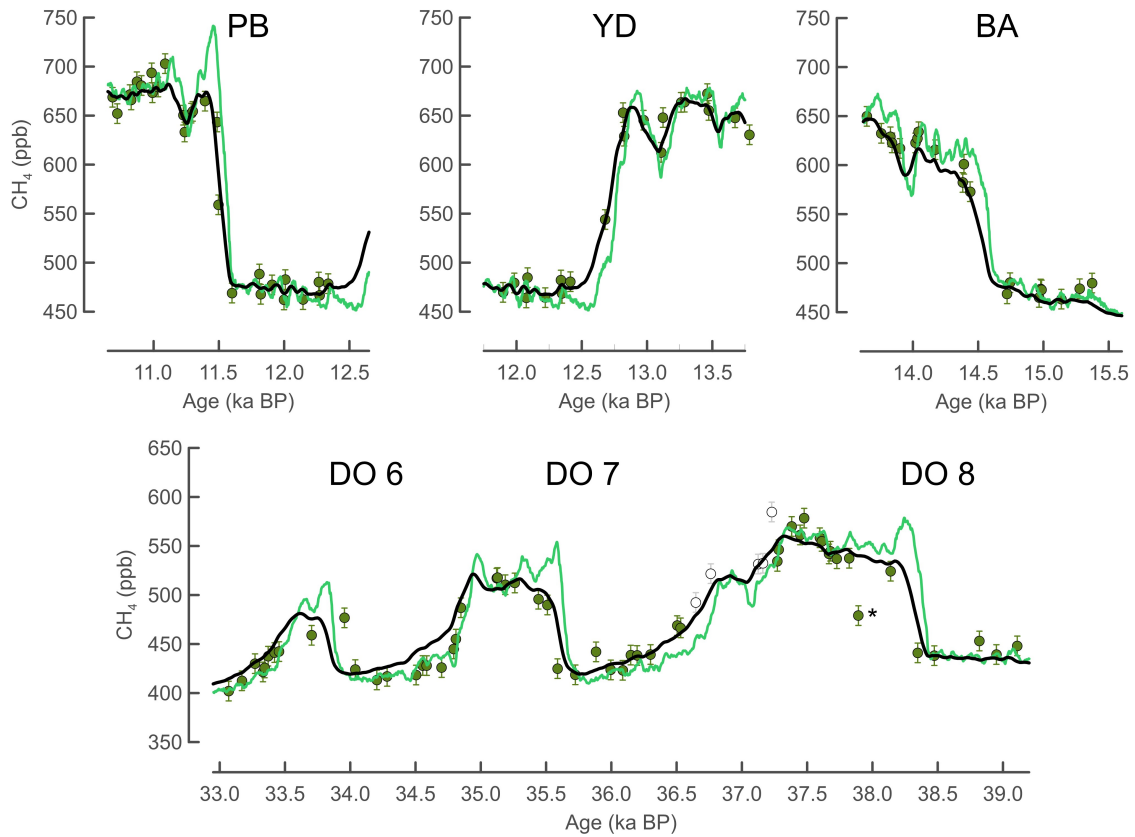


Fig. S5. Abrupt CH₄ transitions at the onsets of four different climatic periods during the last deglaciation and glacial period used for determining Gas Age Distributions (GAD) for the EPICA Dome C (EDC) ice core. These events include the onsets of the Preboreal (PB), Younger Dryas (YD), and Bølling-Allerød (BA) during the last deglaciation (21, 84) and Dansgaard-Oeschger events (DO) 6 - 8 (21, 34) representative for firm column conditions during the colder glacial period. The black lines represent smoothed versions of the continuous West Antarctic Ice Sheet Divide (WD) ice core CH₄ data (light green lines) (18). The smoothed signals shown here (black lines) are produced using the mean values from 500 optimization iterations with the discrete EDC CH₄ data (green dots) varied within their uncertainty boundaries. White points in the lower panel lie outside the 2 ka optimization windows centered around the inflection points of the sharp CH₄ rises. The outlier (*) in the discrete EDC CH₄ data at 37.9 ka BP may be an artefact explained by staggered layering and has been excluded from the optimization runs (81, 82). See materials and methods for details.

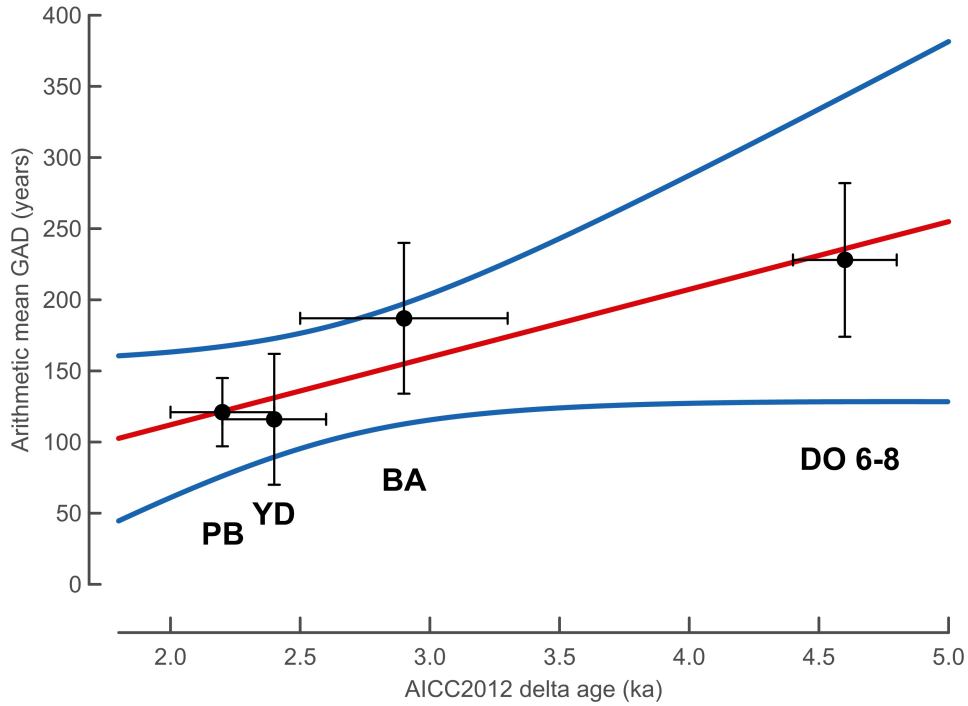


Fig. S6. Linear fit of optimized arithmetic mean values of estimated Gas Age Distributions (GAD) for the EPICA Dome C (EDC) ice core. The arithmetic means are based on a direct comparison between smoothed versions of the continuous CH₄ data from the West Antarctic Ice Sheet Divide (WD) ice core (18) and discrete data from EDC ice core (21, 84) (Fig. S5). The gas-ice difference (delta age) was determined using the AICC2012 age scale (34). Here we focus on the onsets of three key periods, including the Preboreal (PB), Younger Dryas (YD), and Bølling-Allerød (BA) periods all characterized by abrupt CH₄ rises. In addition, we also include Dansgaard-Oeschger events (DO) 6 - 8 representative for firn column conditions during the colder glacial period. The used linear regression model (red line, $R^2=0.85$), including the 95% confidence intervals (blue lines), takes both variable uncertainties (± 2 sigma) into account (86). All GAD are approximated by log-normal functions. See Fig. S5, Eq. S2, and materials and methods for details.

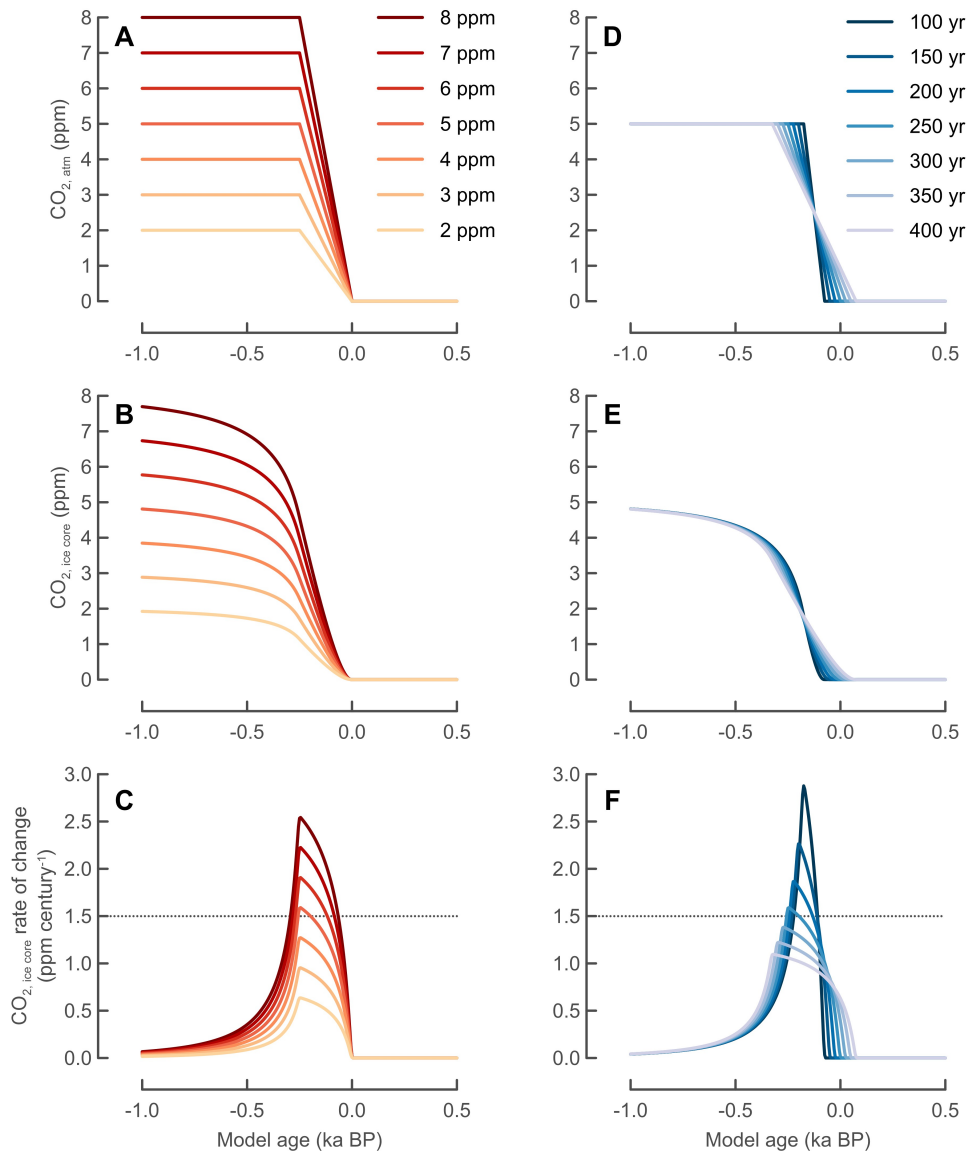


Fig. S7. Detection limit for Carbon Dioxide Jumps (CDJ). (A) Generic CDJ events (i.e., simple step functions) with atmospheric CO₂ rises ranging from 2 to 8 ppm and constant durations of 250 years. (B) Firn column smoothed version of (A) mimicking signals as they would be recorded by the EPICA Dome C ice core during the MIS 12a glacial maximum. MIS 12a represents the coldest interval associated with the strongest firn column-induced smoothing during MIS 9e - 12a. We estimate an arithmetic mean of 233 ± 132 years for the Gas Age Distribution (GAD) at MIS 12a (Eq. S2) based on an estimated delta age of 4.5 ± 0.3 ka (34) (see materials and methods for details). (C) Resulting rate of change of (B), comparable to what would be expected to be found in our ice core record (cf. Fig. S3). (D-F) Same as (A-C) but fixed 5 ppm CO₂ rises and changing durations (100 to 400 years). The dotted lines in (C) and (F) indicate the chosen threshold of 1.5 ppm per century in our CO₂ ice core record analyses (Fig. 1) used to identify CDJ events. See Fig. S8 for a comprehensive matrix of varying combinations of atmospheric CO₂ rises and durations. See supplementary text for details.

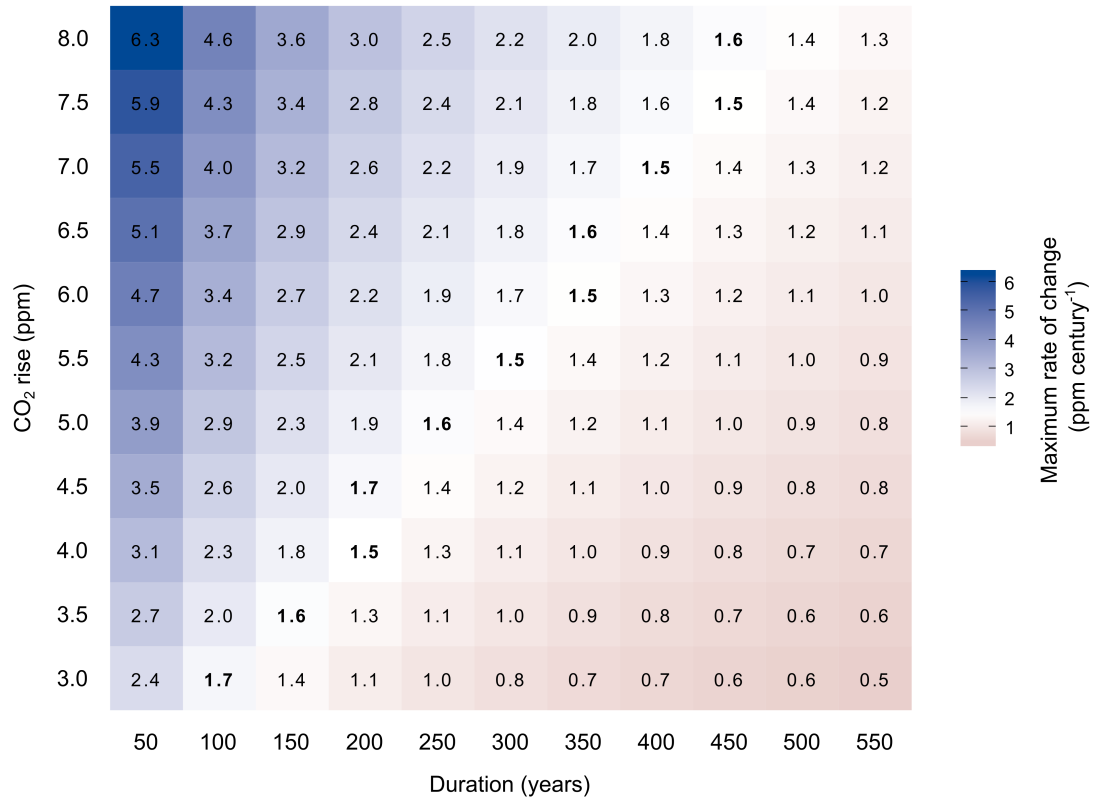


Fig. S8. Heat map of maximum amplitudes in the rates of change of generic Carbon Dioxide Jumps (CDJ) with varying atmospheric CO₂ rises and durations. Generic CDJ with CO₂ rises ranging from 3 to 8 ppm and durations ranging from 50 to 550 years in the atmosphere are smoothed to simulate a signal as it would be archived in the EPICA Dome C (EDC) ice core. Tiles represent peak values of the calculated rate of change of the simulated ice core signal. Identical methodologies to Fig. S7 are used (see supplementary text for details). All combinations of atmospheric CO₂ rises and durations exceeding the threshold value of 1.5 ppm per century in the ice core record would be identified as a CDJ in our EDC CO₂ record. For each magnitude of CO₂ rise (rows) the highest permissible duration that would just allow for CDJ detection is highlighted in bold.

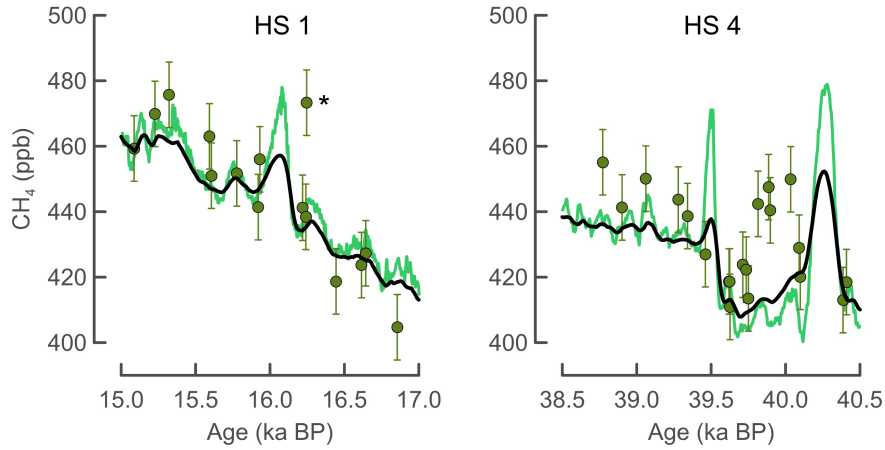


Fig. S9. Smoothing of short-lived overshoots in the CH₄ record in case of the EPICA Dome C (EDC) ice core. An estimation of the EDC firn column-induced smoothing (black line) of short-lived, small amplitude CH₄ overshoots (centered peaks) found in the continuous West Antarctic Ice Sheet Divide (WD) CH₄ record (light green line) for Heinrich Stadials (HS)1 and HS4 (18) during the last glacial period. The WD CH₄ record is smoothed using the linear relationship for EDC gas enclosure characteristics established in Fig. S6 (Eq. S2), assuming a gas-ice age difference (Δ age) of 3.1 ± 0.3 ka and 4.1 ± 0.3 ka (34), resulting in GADs with arithmetic means of 166 ± 103 years (HS1) and 214 ± 123 years (HS4), respectively. Discrete EDC CH₄ data are shown as green dots. Note that mismatches in both records can be explained by age scale inconsistencies. The outlier in the EDC CH₄ record in close proximity to the HS1 WD CH₄ event (*) can likely be explained by staggered layering effects (81, 82) and should not be interpreted as an indicator for reduced smoothing of the EDC ice core.

Event	Duration (years)	CO ₂ rise (ppm)	Growth rate (ppm century ⁻¹)	Delta age (ka)	GAD _{mean} (years)
CDJ+ 9e	59±35	15.8±1.1	26.2±17.6	1.8±0.3	103±82
CDJ- 10a	257±81	12.3±1.9	4.9±1.7	3.3±0.3	175±107
CDJ+ 11a.2	203±160	6.8±1.5	3.4±2.6	2.9±0.3	156±100
CDJ- 11a.2	540±170	10.0±1.8	1.9±0.5	3.0±0.3	161±102
CDJ+ 11a.3	225±176	6.7±1.3	3.0±2.1	2.9±0.3	156±100
CDJ+ 11a.4	140±110	9.3±1.2	6.9±6.7	2.9±0.3	156±100
CDJ- 11c	191±123	12.9±2.7	6.9±5.3	2.1±0.3	118±86
CDJ+ 11e	312±103	9.9±1.7	3.2±1.0	2.2±0.3	123±88

Table S1. Estimated atmospheric characteristics for identified Carbon Dioxide Jumps (CDJ). Estimates are based on empirically-derived gas enclosure (firn smoothing) characteristics for the EPICA Dome C (EDC) ice core, commonly referred to as Gas Age Distributions (GAD). The widths of the GAD (GAD_{mean}) are determined based on the ice-gas age difference (delta age) as derived from the AICC2012 age scale (34). See materials and methods, Fig. 3B, S1B, S6, and Eq. S2 for details. Note that in the case of CDJ+ 11e the duration is likely overestimated whereas the rate of change is likely underestimated. See supplementary text and Fig. S1 for details.

Data S1 (separate file). Antarctic ice core derived CO₂ and CH₄ data from the EPICA Dome C (EDC) ice core covering Marine Isotope Stage 9e - 12a. An additional compilation of the CH₄ data is provided in a separate worksheet. See materials and methods in the supplementary materials for details.

Data S2 (separate file). Marine sediment core derived planktic $\delta^{18}\text{O}$ *G. bulloides* and benthic $\delta^{18}\text{O}$ and $\delta^{13}\text{C}$ *C. wuellerstorfi* from the International Ocean Discovery Program (IODP) Site U1385 covering Marine Isotope Stage 9e - 12a. See materials and methods in the supplementary materials for details.

References and Notes

1. J. R. Petit, J. Jouzel, D. Raynaud, N. I. Barkov, J.-M. Barnola, I. Basile, M. Bender, J. Chappellaz, M. Davis, G. Delaygue, M. Delmotte, V. M. Kotlyakov, M. Legrand, V. Y. Lipenkov, C. Lorius, L. Pépin, C. Ritz, E. Saltzman, M. Stievenard, Climate and atmospheric history of the past 420,000 years from the Vostok ice core, Antarctica. *Nature* **399**, 429–436 (1999). [doi:10.1038/20859](https://doi.org/10.1038/20859)
2. U. Siegenthaler, T. F. Stocker, E. Monnin, D. Lüthi, J. Schwander, B. Stauffer, D. Raynaud, J. M. Barnola, H. Fischer, V. Masson-Delmotte, J. Jouzel, Stable carbon cycle-climate relationship during the Late Pleistocene. *Science* **310**, 1313–1317 (2005). [doi:10.1126/science.1120130](https://doi.org/10.1126/science.1120130) [Medline](#)
3. D. Lüthi, M. Le Floch, B. Bereiter, T. Blunier, J.-M. Barnola, U. Siegenthaler, D. Raynaud, J. Jouzel, H. Fischer, K. Kawamura, T. F. Stocker, High-resolution carbon dioxide concentration record 650,000–800,000 years before present. *Nature* **453**, 379–382 (2008). [doi:10.1038/nature06949](https://doi.org/10.1038/nature06949) [Medline](#)
4. B. Bereiter, D. Lüthi, M. Siegrist, S. Schüpbach, T. F. Stocker, H. Fischer, Mode change of millennial CO₂ variability during the last glacial cycle associated with a bipolar marine carbon seesaw. *Proc. Natl. Acad. Sci. U.S.A.* **109**, 9755–9760 (2012). [doi:10.1073/pnas.1204069109](https://doi.org/10.1073/pnas.1204069109) [Medline](#)
5. J. Ahn, E. J. Brook, Siple Dome ice reveals two modes of millennial CO₂ change during the last ice age. *Nat. Commun.* **5**, 3723 (2014). [doi:10.1038/ncomms4723](https://doi.org/10.1038/ncomms4723) [Medline](#)
6. S. A. Marcott, T. K. Bauska, C. Buizert, E. J. Steig, J. L. Rosen, K. M. Cuffey, T. J. Fudge, J. P. Severinghaus, J. Ahn, M. L. Kalk, J. R. McConnell, T. Sowers, K. C. Taylor, J. W. C. White, E. J. Brook, Centennial-scale changes in the global carbon cycle during the last deglaciation. *Nature* **514**, 616–619 (2014). [doi:10.1038/nature13799](https://doi.org/10.1038/nature13799) [Medline](#)
7. H. Fischer, K. J. Meissner, A. C. Mix, N. J. Abram, J. Austermann, V. Brovkin, E. Capron, D. Colombaroli, A.-L. Daniau, K. A. Dyez, T. Felis, S. A. Finkelstein, S. L. Jaccard, E. L. McClymont, A. Rovere, J. Sutter, E. W. Wolff, S. Affolter, P. Bakker, J. A. Ballesteros-Cánovas, C. Barbante, T. Caley, A. E. Carlson, O. Churakova, G. Cortese, B. F. Cumming, B. A. S. Davis, A. de Vernal, J. Emile-Geay, S. C. Fritz, P. Gierz, J. Gottschalk, M. D. Holloway, F. Joos, M. Kucera, M.-F. Loutre, D. J. Lunt, K. Marcisz, J. R. Marlon, P. Martinez, V. Masson-Delmotte, C. Nehrbass-Ahles, B. L. Otto-Bliesner, C. C. Raible, B. Risebrobakken, M. F. Sánchez Goñi, J. S. Arrigo, M. Sarnthein, J. Sjolte, T. F. Stocker, P. A. Velasquez Álvarez, W. Tinner, P. J. Valdes, H. Vogel, H. Wanner, Q. Yan, Z. Yu, M. Ziegler, L. Zhou, Palaeoclimate constraints on the impact of 2°C anthropogenic warming and beyond. *Nat. Geosci.* **11**, 474–485 (2018). [doi:10.1038/s41561-018-0146-0](https://doi.org/10.1038/s41561-018-0146-0)
8. J. Ahn, E. J. Brook, Atmospheric CO₂ and climate on millennial time scales during the last glacial period. *Science* **322**, 83–85 (2008). [doi:10.1126/science.1160832](https://doi.org/10.1126/science.1160832) [Medline](#)
9. E. Monnin, A. Indermühle, A. Dällenbach, J. Flückiger, B. Stauffer, T. F. Stocker, D. Raynaud, J. M. Barnola, Atmospheric CO₂ concentrations over the last glacial termination. *Science* **291**, 112–114 (2001). [doi:10.1126/science.291.5501.112](https://doi.org/10.1126/science.291.5501.112) [Medline](#)
10. J. Jouzel, V. Masson-Delmotte, O. Cattani, G. Dreyfus, S. Falourd, G. Hoffmann, B. Minster, J. Nouet, J. M. Barnola, J. Chappellaz, H. Fischer, J. C. Gallet, S. Johnsen, M. Leuenberger, L. Loulergue, D. Luethi, H. Oerter, F. Parrenin, G. Raisbeck, D.

- Raynaud, A. Schilt, J. Schwander, E. Selmo, R. Souchez, R. Spahni, B. Stauffer, J. P. Steffensen, B. Stenni, T. F. Stocker, J. L. Tison, M. Werner, E. W. Wolff, Orbital and millennial Antarctic climate variability over the past 800,000 years. *Science* **317**, 793–796 (2007). [doi:10.1126/science.1141038](https://doi.org/10.1126/science.1141038) [Medline](#)
11. T. F. Stocker, S. J. Johnsen, A minimum thermodynamic model for the bipolar seesaw. *Paleoceanography* **18**, 1087 (2003). [doi:10.1029/2003PA000920](https://doi.org/10.1029/2003PA000920)
 12. J. Ahn, E. J. Brook, A. Schmittner, K. Kreutz, Abrupt change in atmospheric CO₂ during the last ice age. *Geophys. Res. Lett.* **39**, 5 (2012). [doi:10.1029/2012GL053018](https://doi.org/10.1029/2012GL053018)
 13. T. K. Bauska, E. J. Brook, S. A. Marcott, D. Baggenstos, S. Shackleton, J. P. Severinghaus, V. V. Petrenko, Controls on millennial-scale atmospheric CO₂ variability during the last glacial period. *Geophys. Res.* **45**, 7731–7740 (2018). [doi:10.1029/2018GL077881](https://doi.org/10.1029/2018GL077881)
 14. S. R. Hemming, Heinrich events: Massive late Pleistocene detritus layers of the North Atlantic and their global climate imprint. *Rev. Geophys.* **42**, RG1005 (2004). [doi:10.1029/2003RG000128](https://doi.org/10.1029/2003RG000128)
 15. L. G. Henry, J. F. McManus, W. B. Curry, N. L. Roberts, A. M. Piotrowski, L. D. Keigwin, North Atlantic ocean circulation and abrupt climate change during the last glaciation. *Science* **353**, 470–474 (2016). [doi:10.1126/science.aaf5529](https://doi.org/10.1126/science.aaf5529) [Medline](#)
 16. Heinrich stadials are directly linked to massive glacial ice and meltwater discharges from the Hudson Strait known as Heinrich events.
 17. M. Baumgartner, P. Kindler, O. Eicher, G. Floch, A. Schilt, J. Schwander, R. Spahni, E. Capron, J. Chappellaz, M. Leuenberger, H. Fischer, T. F. Stocker, NGRIP CH₄ concentration from 120 to 10 kyr before present and its relation to a $\delta^{15}\text{N}$ temperature reconstruction from the same ice core. *Clim. Past* **10**, 903–920 (2014). [doi:10.5194/cp-10-903-2014](https://doi.org/10.5194/cp-10-903-2014)
 18. R. H. Rhodes, E. J. Brook, J. C. H. Chiang, T. Blunier, O. J. Maselli, J. R. McConnell, D. Romanini, J. P. Severinghaus, Enhanced tropical methane production in response to iceberg discharge in the North Atlantic. *Science* **348**, 1016–1019 (2015). [doi:10.1126/science.1262005](https://doi.org/10.1126/science.1262005) [Medline](#)
 19. L. B. Railsback, P. L. Gibbard, M. J. Head, N. R. G. Voarintsoa, S. Toucanne, An optimized scheme of lettered marine isotope substages for the last 1.0 million years, and the climatostratigraphic nature of isotope stages and substages. *Quat. Sci. Rev.* **111**, 94–106 (2015). [doi:10.1016/j.quascirev.2015.01.012](https://doi.org/10.1016/j.quascirev.2015.01.012)
 20. Materials and methods are available as supplementary materials.
 21. L. Loulergue, A. Schilt, R. Spahni, V. Masson-Delmotte, T. Blunier, B. Lemieux, J.-M. Barnola, D. Raynaud, T. F. Stocker, J. Chappellaz, Orbital and millennial-scale features of atmospheric CH₄ over the past 800,000 years. *Nature* **453**, 383–386 (2008). [doi:10.1038/nature06950](https://doi.org/10.1038/nature06950) [Medline](#)
 22. Benthic $\delta^{13}\text{C}$ of *C. wuellerstorfi* reflects changes in deep-water ventilation related to reorganization of deep-ocean circulation and remineralization of organic carbon. The $\delta^{18}\text{O}$ signal of the same species indicates variations in deep-water temperatures.
 23. Millennial-scale changes in the planktic $\delta^{18}\text{O}$ record of *G. bulloides* follow changes in the sea surface temperature in the North Atlantic.

24. P. C. Tzedakis, D. Raynaud, J. F. McManus, A. Berger, V. Brovkin, T. Kiefer, Interglacial diversity. *Nat. Geosci.* **2**, 751–755 (2009). [doi:10.1038/ngeo660](https://doi.org/10.1038/ngeo660)
25. P. C. Tzedakis, E. W. Wolff, L. C. Skinner, V. Brovkin, D. A. Hodell, J. F. McManus, D. Raynaud, Can we predict the duration of an interglacial? *Clim. Past* **8**, 1473–1485 (2012). [doi:10.5194/cp-8-1473-2012](https://doi.org/10.5194/cp-8-1473-2012)
26. T. Rodrigues, M. Alonso-García, D. A. Hodell, M. Rufino, F. Naughton, J. O. Grimalt, A. H. L. Voelker, F. Abrantes, A 1-Ma record of sea surface temperature and extreme cooling events in the North Atlantic: A perspective from the Iberian Margin. *Quat. Sci. Rev.* **172**, 118–130 (2017). [doi:10.1016/j.quascirev.2017.07.004](https://doi.org/10.1016/j.quascirev.2017.07.004)
27. F. Lambert, M. Bigler, J. P. Steffensen, M. Hutterli, H. Fischer, Centennial mineral dust variability in high-resolution ice core data from Dome C, Antarctica. *Clim. Past* **8**, 609–623 (2012). [doi:10.5194/cp-8-609-2012](https://doi.org/10.5194/cp-8-609-2012)
28. N. J. Shackleton, M. A. Hall, E. Vincent, Phase relationships between millennial-scale events 64,000–24,000 years ago. *Paleoceanography* **15**, 565–569 (2000). [doi:10.1029/2000PA000513](https://doi.org/10.1029/2000PA000513)
29. R. Schneider, J. Schmitt, P. Köhler, F. Joos, H. Fischer, A reconstruction of atmospheric carbon dioxide and its stable carbon isotopic composition from the penultimate glacial maximum to the last glacial inception. *Clim. Past* **9**, 2507–2523 (2013). [doi:10.5194/cp-9-2507-2013](https://doi.org/10.5194/cp-9-2507-2013)
30. T. K. Bauska, D. Baggenstos, E. J. Brook, A. C. Mix, S. A. Marcott, V. V. Petrenko, H. Schaefer, J. P. Severinghaus, J. E. Lee, Carbon isotopes characterize rapid changes in atmospheric carbon dioxide during the last deglaciation. *Proc. Natl. Acad. Sci. U.S.A.* **113**, 3465–3470 (2016). [doi:10.1073/pnas.1513868113](https://doi.org/10.1073/pnas.1513868113) [Medline](#)
31. F. Joos, R. Spahni, Rates of change in natural and anthropogenic radiative forcing over the past 20,000 years. *Proc. Natl. Acad. Sci. U.S.A.* **105**, 1425–1430 (2008). [doi:10.1073/pnas.0707386105](https://doi.org/10.1073/pnas.0707386105) [Medline](#)
32. P. Tans, R. Keeling, Annual mean CO₂ growth rate for Mauna Loa, Hawaii (NOAA/ESRL and Scripps Institution of Oceanography, 2020); www.esrl.noaa.gov/gmd/ccgg/trends/gr.html.
33. T. Extier, A. Landais, C. Bréant, F. Prié, L. Bazin, G. Dreyfus, D. M. Roche, M. Leuenberger, On the use of $\delta^{18}\text{O}_{\text{atm}}$ for ice core dating. *Quat. Sci. Rev.* **185**, 244–257 (2018). [doi:10.1016/j.quascirev.2018.02.008](https://doi.org/10.1016/j.quascirev.2018.02.008)
34. L. Bazin, A. Landais, B. Lemieux-Dudon, H. Toyé Mahamadou Kele, D. Veres, F. Parrenin, P. Martinerie, C. Ritz, E. Capron, V. Lipenkov, M.-F. Loutre, D. Raynaud, B. Vinther, A. Svensson, S. O. Rasmussen, M. Severi, T. Blunier, M. Leuenberger, H. Fischer, V. Masson-Delmotte, J. Chappellaz, E. Wolff, An optimized multi-proxy, multi-site Antarctic ice and gas orbital chronology (AICC2012): 120–800 ka. *Clim. Past* **9**, 1715–1731 (2013). [doi:10.5194/cp-9-1715-2013](https://doi.org/10.5194/cp-9-1715-2013)
35. H. Cheng, R. L. Edwards, A. Sinha, C. Spötl, L. Yi, S. Chen, M. Kelly, G. Kathayat, X. Wang, X. Li, X. Kong, Y. Wang, Y. Ning, H. Zhang, The Asian monsoon over the past 640,000 years and ice age terminations. *Nature* **534**, 640–646 (2016). [doi:10.1038/nature18591](https://doi.org/10.1038/nature18591) [Medline](#)
36. A. Bozbiyik, M. Steinacher, F. Joos, T. F. Stocker, L. Menviel, Fingerprints of changes in the terrestrial carbon cycle in response to large reorganizations in ocean circulation. *Clim. Past* **7**, 319–338 (2011). [doi:10.5194/cp-7-319-2011](https://doi.org/10.5194/cp-7-319-2011)

37. R. M. Spratt, L. E. Lisiecki, A Late Pleistocene sea level stack. *Clim. Past* **12**, 1079–1092 (2016). [doi:10.5194/cp-12-1079-2016](https://doi.org/10.5194/cp-12-1079-2016)
38. S. Barker, J. Chen, X. Gong, L. Jonkers, G. Knorr, D. Thornalley, Icebergs not the trigger for North Atlantic cold events. *Nature* **520**, 333–336 (2015). [doi:10.1038/nature14330](https://doi.org/10.1038/nature14330) [Medline](#)
39. A. J. Dickson, C. J. Beer, C. Dempsey, M. A. Maslin, J. A. Bendle, E. L. McClymont, R. D. Pancost, Oceanic forcing of the Marine Isotope Stage 11 interglacial. *Nat. Geosci.* **2**, 428–433 (2009). [doi:10.1038/ngeo527](https://doi.org/10.1038/ngeo527)
40. R. G. Hatfield, A. V. Reyes, J. S. Stoner, A. E. Carlson, B. L. Beard, K. Winsor, B. Welke, Interglacial responses of the southern Greenland ice sheet over the last 430,000 years determined using particle-size specific magnetic and isotopic tracers. *Earth Planet. Sci. Lett.* **454**, 225–236 (2016). [doi:10.1016/j.epsl.2016.09.014](https://doi.org/10.1016/j.epsl.2016.09.014)
41. D. J. Wilson, R. A. Bertram, E. F. Needham, T. van de Flierdt, K. J. Welsh, R. M. McKay, A. Mazumder, C. R. Riesselman, F. J. Jimenez-Espejo, C. Escutia, Ice loss from the East Antarctic Ice Sheet during late Pleistocene interglacials. *Nature* **561**, 383–386 (2018). [doi:10.1038/s41586-018-0501-8](https://doi.org/10.1038/s41586-018-0501-8) [Medline](#)
42. J. B. Pedro, M. Jochum, C. Buizert, F. He, S. Barker, S. O. Rasmussen, Beyond the bipolar seesaw: Toward a process understanding of interhemispheric coupling. *Quat. Sci. Rev.* **192**, 27–46 (2018). [doi:10.1016/j.quascirev.2018.05.005](https://doi.org/10.1016/j.quascirev.2018.05.005)
43. T. Chen, L. F. Robinson, A. Burke, J. Southon, P. Spooner, P. J. Morris, H. C. Ng, Synchronous centennial abrupt events in the ocean and atmosphere during the last deglaciation. *Science* **349**, 1537–1541 (2015). [doi:10.1126/science.aac6159](https://doi.org/10.1126/science.aac6159) [Medline](#)
44. S. L. Jaccard, E. D. Galbraith, A. Martínez-García, R. F. Anderson, Covariation of deep Southern Ocean oxygenation and atmospheric CO₂ through the last ice age. *Nature* **530**, 207–210 (2016). [doi:10.1038/nature16514](https://doi.org/10.1038/nature16514) [Medline](#)
45. C. Basak, H. Fröllje, F. Lamy, R. Gersonde, V. Benz, R. F. Anderson, M. Molina-Kescher, K. Pahnke, Breakup of last glacial deep stratification in the South Pacific. *Science* **359**, 900–904 (2018). [doi:10.1126/science.aao2473](https://doi.org/10.1126/science.aao2473) [Medline](#)
46. B. B. Stephens, R. F. Keeling, The influence of Antarctic sea ice on glacial-interglacial CO₂ variations. *Nature* **404**, 171–174 (2000). [doi:10.1038/35004556](https://doi.org/10.1038/35004556) [Medline](#)
47. A. Schmittner, E. D. Galbraith, Glacial greenhouse-gas fluctuations controlled by ocean circulation changes. *Nature* **456**, 373–376 (2008). [doi:10.1038/nature07531](https://doi.org/10.1038/nature07531) [Medline](#)
48. M. Lacerra, D. Lund, J. Yu, A. Schmittner, Carbon storage in the mid-depth Atlantic during millennial-scale climate events. *Paleoceanography* **32**, 780–795 (2017). [doi:10.1002/2016PA003081](https://doi.org/10.1002/2016PA003081)
49. L. Menviel, P. Spence, J. Yu, M. A. Chamberlain, R. J. Matear, K. J. Meissner, M. H. England, Southern Hemisphere westerlies as a driver of the early deglacial atmospheric CO₂ rise. *Nat. Commun.* **9**, 2503 (2018). [doi:10.1038/s41467-018-04876-4](https://doi.org/10.1038/s41467-018-04876-4) [Medline](#)
50. J. W. B. Rae, A. Burke, L. F. Robinson, J. F. Adkins, T. Chen, C. Cole, R. Greenop, T. Li, E. F. M. Littley, D. C. Nita, J. A. Stewart, B. J. Taylor, CO₂ storage and release in the deep Southern Ocean on millennial to centennial timescales. *Nature* **562**, 569–573 (2018). [doi:10.1038/s41586-018-0614-0](https://doi.org/10.1038/s41586-018-0614-0) [Medline](#)

51. P. Köhler, G. Knorr, E. Bard, Permafrost thawing as a possible source of abrupt carbon release at the onset of the Bølling/Allerød. *Nat. Commun.* **5**, 5520 (2014).
[doi:10.1038/ncomms6520](https://doi.org/10.1038/ncomms6520) [Medline](#)
52. A. Jeltsch-Thömmes, F. Joos, Modeling the evolution of pulse-like perturbations in atmospheric carbon and carbon isotopes: The role of weathering–sedimentation imbalances. *Clim. Past* **16**, 423–451 (2020). [doi:10.5194/cp-16-423-2020](https://doi.org/10.5194/cp-16-423-2020)
53. C. Buizert, M. Sigl, M. Severi, B. R. Markle, J. J. Wettstein, J. R. McConnell, J. B. Pedro, H. Sodemann, K. Goto-Azuma, K. Kawamura, S. Fujita, H. Motoyama, M. Hirabayashi, R. Uemura, B. Stenni, F. Parrenin, F. He, T. J. Fudge, E. J. Steig, Abrupt ice-age shifts in southern westerly winds and Antarctic climate forced from the north. *Nature* **563**, 681–685 (2018). [doi:10.1038/s41586-018-0727-5](https://doi.org/10.1038/s41586-018-0727-5) [Medline](#)
54. P. U. Clark, J. D. Shakun, S. A. Marcott, A. C. Mix, M. Eby, S. Kulp, A. Levermann, G. A. Milne, P. L. Pfister, B. D. Santer, D. P. Schrag, S. Solomon, T. F. Stocker, B. H. Strauss, A. J. Weaver, R. Winkelmann, D. Archer, E. Bard, A. Goldner, K. Lambeck, R. T. Pierrehumbert, G.-K. Plattner, Consequences of twenty-first-century policy for multi-millennial climate and sea-level change. *Nat. Clim. Chang.* **6**, 360–369 (2016).
[doi:10.1038/nclimate2923](https://doi.org/10.1038/nclimate2923)
55. C. Nehrbass-Ahles, J. Shin, J. Schmitt, B. Bereiter, F. Joos, A. Schilt, L. Schmidely, L. Silva, G. Teste, R. Grilli, J. A. Chappellaz, D. A. Hodell, H. Fischer, T. Stocker, High-resolution atmospheric CO₂ and CH₄ records derived from the EPICA Dome C ice core and stable isotope records from marine sediment core IODP Site U1385 covering MIS 9e - 12a, PANGAEA (2020);
<https://doi.org/10.1594/PANGAEA.915146>.
56. B. Bereiter, T. F. Stocker, H. Fischer, A centrifugal ice microtome for measurements of atmospheric CO₂ on air trapped in polar ice cores. *Atmos. Meas. Tech.* **6**, 251–262 (2013). [doi:10.5194/amt-6-251-2013](https://doi.org/10.5194/amt-6-251-2013)
57. P. P. Tans, A. M. Crotwell, K. W. Thoning, Abundances of isotopologues and calibration of CO₂ greenhouse gas measurements. *Atmos. Meas. Tech.* **10**, 2669–2685 (2017).
[doi:10.5194/amt-10-2669-2017](https://doi.org/10.5194/amt-10-2669-2017)
58. H. Schaefer, A. Lourantou, J. Chappellaz, D. Lüthi, B. Bereiter, J.-M. Barnola, On the suitability of partially clathrated ice for analysis of concentration and $\delta^{13}\text{C}$ of palaeo-atmospheric CO₂. *Earth Planet. Sci. Lett.* **307**, 334–340 (2011).
[doi:10.1016/j.epsl.2011.05.007](https://doi.org/10.1016/j.epsl.2011.05.007)
59. A. Schilt, M. Baumgartner, T. Blunier, J. Schwander, R. Spahni, H. Fischer, T. F. Stocker, Glacial–interglacial and millennial-scale variations in the atmospheric nitrous oxide concentration during the last 800,000 years. *Quat. Sci. Rev.* **29**, 182–192 (2010). [doi:10.1016/j.quascirev.2009.03.011](https://doi.org/10.1016/j.quascirev.2009.03.011)
60. R. Spahni, J. Chappellaz, T. F. Stocker, L. Loulergue, G. Hausammann, K. Kawamura, J. Flückiger, J. Schwander, D. Raynaud, V. Masson-Delmotte, J. Jouzel, Atmospheric methane and nitrous oxide of the Late Pleistocene from Antarctic ice cores. *Science* **310**, 1317–1321 (2005). [doi:10.1126/science.1120132](https://doi.org/10.1126/science.1120132) [Medline](#)
61. M. Bock, J. Schmitt, J. Beck, B. Seth, J. Chappellaz, H. Fischer, Glacial/interglacial wetland, biomass burning, and geologic methane emissions constrained by dual stable isotopic CH₄ ice core records. *Proc. Natl. Acad. Sci. U.S.A.* **114**, E5778–E5786 (2017). [doi:10.1073/pnas.1613883114](https://doi.org/10.1073/pnas.1613883114) [Medline](#)

62. D. Hodell, L. Lourens, S. Crowhurst, T. Konijnendijk, R. Tjallingii, F. Jiménez-Espejo, L. Skinner, P. C. Tzedakis, F. Abrantes, G. D. Acton, C. A. Alvarez Zarikian, A. Bahr, B. Balestra, E. L. Barranco, G. Carrara, E. Ducassou, R. D. Flood, J.-A. Flores, S. Furota, J. Grimalt, P. Grunert, J. Hernández-Molina, J. K. Kim, L. A. Krissek, J. Kuroda, B. Li, J. Lofi, V. Margari, B. Martrat, M. D. Miller, F. Nanayama, N. Nishida, C. Richter, T. Rodrigues, F. J. Rodríguez-Tovar, A. C. F. Roque, M. F. Sanchez Goñi, F. J. Sierro Sánchez, A. D. Singh, C. R. Sloss, D. A. V. Stow, Y. Takashimizu, A. Tzanova, A. Voelker, C. Xuan, T. Williams, A reference time scale for Site U1385 (Shackleton Site) on the SW Iberian Margin. *Global Planet. Change* **133**, 49–64 (2015). [doi:10.1016/j.gloplacha.2015.07.002](https://doi.org/10.1016/j.gloplacha.2015.07.002)
63. N. J. Shackleton, R. G. Fairbanks, T.-C. Chiu, F. Parrenin, Absolute calibration of the Greenland time scale: Implications for Antarctic time scales and for $\Delta^{14}\text{C}$. *Quat. Sci. Rev.* **23**, 1513–1522 (2004). [doi:10.1016/j.quascirev.2004.03.006](https://doi.org/10.1016/j.quascirev.2004.03.006)
64. B. Martrat, J. O. Grimalt, N. J. Shackleton, L. de Abreu, M. A. Hutterli, T. F. Stocker, Four climate cycles of recurring deep and surface water destabilizations on the Iberian margin. *Science* **317**, 502–507 (2007). [doi:10.1126/science.1139994](https://doi.org/10.1126/science.1139994) [Medline](#)
65. L. C. Skinner, H. Elderfield, Rapid fluctuations in the deep North Atlantic heat budget during the last glacial period. *Paleoceanography* **22**, PA1205 (2007). [doi:10.1029/2006PA001338](https://doi.org/10.1029/2006PA001338)
66. P. C. Tzedakis, K. H. Roucoux, L. de Abreu, N. J. Shackleton, The duration of forest stages in southern Europe and interglacial climate variability. *Science* **306**, 2231–2235 (2004). [doi:10.1126/science.1102398](https://doi.org/10.1126/science.1102398) [Medline](#)
67. S. Barker, G. Knorr, R. L. Edwards, F. Parrenin, A. E. Putnam, L. C. Skinner, E. Wolff, M. Ziegler, 800,000 years of abrupt climate variability. *Science* **334**, 347–351 (2011). [doi:10.1126/science.1203580](https://doi.org/10.1126/science.1203580) [Medline](#)
68. H. Craig, Y. Horibe, T. Sowers, Gravitational separation of gases and isotopes in polar ice caps. *Science* **242**, 1675–1678 (1988). [doi:10.1126/science.242.4886.1675](https://doi.org/10.1126/science.242.4886.1675) [Medline](#)
69. T. Sowers, M. Bender, D. Raynaud, Elemental and isotopic composition of occluded O_2 and N_2 in polar ice. *J. Geophys. Res.* **94**, 5137–5150 (1989). [doi:10.1029/JD094iD04p05137](https://doi.org/10.1029/JD094iD04p05137)
70. D. M. Etheridge, L. P. Steele, R. L. Langenfelds, R. J. Francey, J.-M. Barnola, V. I. Morgan, Natural and anthropogenic changes in atmospheric CO_2 over the last 1000 years from air in Antarctic ice and firn. *J. Geophys. Res. Atmos.* **101**, 4115–4128 (1996). [doi:10.1029/95JD03410](https://doi.org/10.1029/95JD03410)
71. S. Eggleston, J. Schmitt, B. Bereiter, R. Schneider, H. Fischer, Evolution of the stable carbon isotope composition of atmospheric CO_2 over the last glacial cycle. *Paleoceanography* **31**, 434–452 (2016). [doi:10.1002/2015PA002874](https://doi.org/10.1002/2015PA002874)
72. G. B. Dreyfus, J. Jouzel, M. L. Bender, A. Landais, V. Masson-Delmotte, M. Leuenberger, Firn processes and $\delta^{15}\text{N}$: Potential for a gas-phase climate proxy. *Quat. Sci. Rev.* **29**, 28–42 (2010). [doi:10.1016/j.quascirev.2009.10.012](https://doi.org/10.1016/j.quascirev.2009.10.012)
73. M. L. Bender, Orbital tuning chronology for the Vostok climate record supported by trapped gas composition. *Earth Planet. Sci. Lett.* **204**, 275–289 (2002). [doi:10.1016/S0012-821X\(02\)00980-9](https://doi.org/10.1016/S0012-821X(02)00980-9)
74. B. Bereiter, S. Eggleston, J. Schmitt, C. Nehrbass-Ahles, T. F. Stocker, H. Fischer, S. Kipfstuhl, J. Chappellaz, Revision of the EPICA Dome C CO_2 record from 800 to 600

- kyr before present. *Geophys. Res. Lett.* **42**, 542–549 (2015).
[doi:10.1002/2014GL061957](https://doi.org/10.1002/2014GL061957)
75. P. Köhler, C. Nehrbass-Ahles, J. Schmitt, T. F. Stocker, H. Fischer, A 156 kyr smoothed history of the atmospheric greenhouse gases CO₂, CH₄, and N₂O and their radiative forcing. *Earth Syst. Sci. Data* **9**, 363–387 (2017). [doi:10.5194/essd-9-363-2017](https://doi.org/10.5194/essd-9-363-2017)
 76. I. G. Enting, On the use of smoothing splines to filter CO₂ data. *J. Geophys. Res. Atmos.* **92**, 10977–10984 (1987). [doi:10.1029/JD092iD09p10977](https://doi.org/10.1029/JD092iD09p10977)
 77. J. Schwander, B. Stauffer, Age difference between polar ice and the air trapped in its bubbles. *Nature* **311**, 45–47 (1984). [doi:10.1038/311045a0](https://doi.org/10.1038/311045a0)
 78. R. Spahni, J. Schwander, J. Flückiger, B. Stauffer, J. Chappellaz, D. Raynaud, The attenuation of fast atmospheric CH₄ variations recorded in polar ice cores. *Geophys. Res. Lett.* **30**, 1571 (2003). [doi:10.1029/2003GL017093](https://doi.org/10.1029/2003GL017093)
 79. C. Buizert, P. Martinerie, V. V. Petrenko, J. P. Severinghaus, C. M. Trudinger, E. Witrant, J. L. Rosen, A. J. Orsi, M. Rubino, D. M. Etheridge, L. P. Steele, C. Hogan, J. C. Laube, W. T. Sturges, V. A. Levchenko, A. M. Smith, I. Levin, T. J. Conway, E. J. Dlugokencky, P. M. Lang, K. Kawamura, T. M. Jenk, J. W. C. White, T. Sowers, J. Schwander, T. Blunier, Gas transport in firn: Multiple-tracer characterisation and model intercomparison for NEEM, Northern Greenland. *Atmos. Chem. Phys.* **12**, 4259–4277 (2012). [doi:10.5194/acp-12-4259-2012](https://doi.org/10.5194/acp-12-4259-2012)
 80. P. Köhler, G. Knorr, D. Buiron, A. Lourantou, J. Chappellaz, Abrupt rise in atmospheric CO₂ at the onset of the Bølling/Allerød: In-situ ice core data versus true atmospheric signals. *Clim. Past* **7**, 473–486 (2011). [doi:10.5194/cp-7-473-2011](https://doi.org/10.5194/cp-7-473-2011)
 81. K. Fourteau, X. Faïn, P. Martinerie, A. Landais, A. A. Ekaykin, V. Y. Lipenkov, J. Chappellaz, Analytical constraints on layered gas trapping and smoothing of atmospheric variability in ice under low-accumulation conditions. *Clim. Past* **13**, 1815–1830 (2017). [doi:10.5194/cp-13-1815-2017](https://doi.org/10.5194/cp-13-1815-2017)
 82. R. H. Rhodes, X. Faïn, E. J. Brook, J. R. McConnell, O. J. Maselli, M. Sigl, J. Edwards, C. Buizert, T. Blunier, J. Chappellaz, J. Freitag, Local artifacts in ice core methane records caused by layered bubble trapping and in situ production: A multi-site investigation. *Clim. Past* **12**, 1061–1077 (2016). [doi:10.5194/cp-12-1061-2016](https://doi.org/10.5194/cp-12-1061-2016)
 83. S. Bihorel, M. Baudin, “R Port of the ‘Scilab’ Neldermead Module,” Version 1.0-11 (2018); <https://cran.r-project.org/web/packages/neldermead/neldermead.pdf>.
 84. F. Parrenin, V. Masson-Delmotte, P. Köhler, D. Raynaud, D. Paillard, J. Schwander, C. Barbante, A. Landais, A. Wegner, J. Jouzel, Synchronous change of atmospheric CO₂ and Antarctic temperature during the last deglacial warming. *Science* **339**, 1060–1063 (2013). [doi:10.1126/science.1226368](https://doi.org/10.1126/science.1226368) [Medline](#)
 85. C. Buizert, K. M. Cuffey, J. P. Severinghaus, D. Baggenstos, T. J. Fudge, E. J. Steig, B. R. Markle, M. Winstrup, R. H. Rhodes, E. J. Brook, T. A. Sowers, G. D. Clow, H. Cheng, R. L. Edwards, M. Sigl, J. R. McConnell, K. C. Taylor, The WAIS Divide deep ice core WD2014 chronology – Part 1: Methane synchronization (68–31 ka BP) and the gas age-ice age difference. *Clim. Past* **11**, 153–173 (2015). [doi:10.5194/cp-11-153-2015](https://doi.org/10.5194/cp-11-153-2015)
 86. D. York, Least-squares fitting of a straight line. *Can. J. Phys.* **44**, 1079–1086 (1966).
[doi:10.1139/p66-090](https://doi.org/10.1139/p66-090)

87. D. Lüthi, B. Bereiter, B. Stauffer, R. Winkler, J. Schwander, P. Kindler, M. Leuenberger, S. Kipfstuhl, E. Capron, A. Landais, H. Fischer, T. F. Stocker, CO₂ and O₂/N₂ variations in and just below the bubble–clathrate transformation zone of Antarctic ice cores. *Earth Planet. Sci. Lett.* **297**, 226–233 (2010). [doi:10.1016/j.epsl.2010.06.023](https://doi.org/10.1016/j.epsl.2010.06.023)